INFLUENCE OF ELASTIC SUPPORTS ON THE DYNAMIC RESPONSE OF TWO RAILS CONNECTED WITH JOINT BARS

Traian MAZILU[1], Marius-Alin GHEȚI[2], Mihai-Cornel LEU[3]

In this paper, the influence of elastic supports on the dynamic behaviour of the two rails connected through two joint bars is presented aiming to point out the design requirements for supports to allow identification of the damping of the rails-joint bars connection via a test rig. To this end, the test rig model consisting of two Euler-Bernoulli beams (rails) connected with an equivalent beam (joint bars) is proposed. The test rig and experimental results in terms of rail receptance are shown and analysed. The stiffness and damping of the supports and rails-joint bars connection are identified based on comparison between the experiment out comes and theoretical results from the model. Using this model, the influence of the gap length is revealed.

Keywords: rail joint, joint bar, Euler-Bernoulli beam, impact hammer method, stiffness, hysteretic damping

1. Introduction

Nowadays, the jointed track still represents the most common solution for the secondary railway lines, where the speed and traffic are reduced, due to the low cost of construction and unsophisticated maintenance equipment.

Figure 1 illustrates the main characteristic of a jointed track, namely the rail joint. Two rails of standard length (usually, 12, 15, 22.5, 25 or 30 m) are assembled by means of a joint consisting of two joint bars fixed by means of four bolts. A small gap of maximum 20 mm length at -16 °C [1] secures rails against the buckling.

Running along a jointed track, the vehicles experience shocks and specific noise affecting the ride quality and ride comfort. To improve the construction and performance of the jointed track many theoretical and experimental studies have been performed.

[1]Prof., Department of Railway Vehicles, University Politehnica of Bucharest, Romania, e-mail: traian.mazilu@upb.ro
[2]Ass. Prof. PhD Student, Department of Railway Vehicles, University Politehnica of Bucharest, Romania, e-mail: marius.gheti@upb.ro
[3] PhD Student, Doctoral School of Transport, University Politehnica of Bucharest, e-mail: mihaileu.c@gmail.com

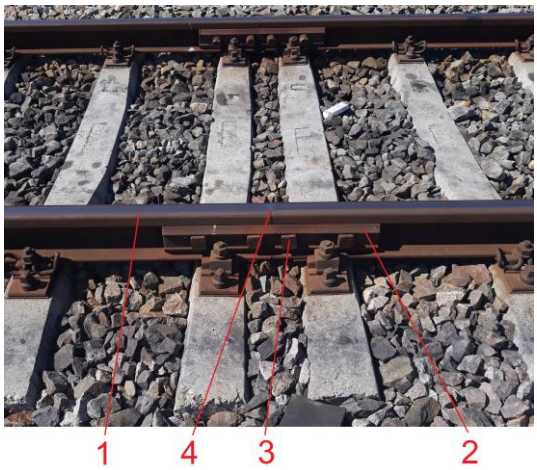

Fig. 1. Jointing rails: 1. rail end; 2. joint bar; 3. bolt; 4. gap.

The structural integrity and deflection performance of a bolted rail joint under static loading has been studied using a three-dimensional finite element method [2]. Using an explicit finite element wheel-IRJ dynamic interaction model, the high-frequency impact vibration and noise generated at a typical IRJ in the Dutch railway network has been studied [3]. Other related aspects such the elasto-plastic field [4], the surface wear at the rail joint [5] have been addressed. Many experimental researches in situ have been performed to validate the theoretical models [3, 6].

In this paper, a different experimental approach is proposed to validate the rail joint model, namely using a test rig consisting of two rails connected with two joint bars and bolts resting on elastic foundation. According to the test rig structure, the rail joint model has three finite length Euler-Bernoulli beams: two identic beams model the rails and the third one is equivalent to the two joint bars. Rails – joint bars connection is modelled using Winkler foundation. Test rig design is based on the theoretical outcomes from the study of influence of elastic supports on the dynamic response of two rails connected with joint bars. Starting from the experimental results obtained via the impact hammer method, the stiffness and hysteretic damping of the test rig foundation and rails-joint bars connection are determined.

2. Test rig and experimental results

Figure 2 shows the test rig used to determine the frequency response function of the two rails – joint bars system using the impact hammer method. The system consists of 2 rails of 598 mm each, connected with two rail joint bars of 615 mm, which rest on elastic supports at the ends. Rails and rail joint bars correspond to 49 rail type.

Fig. 2. Test rig.

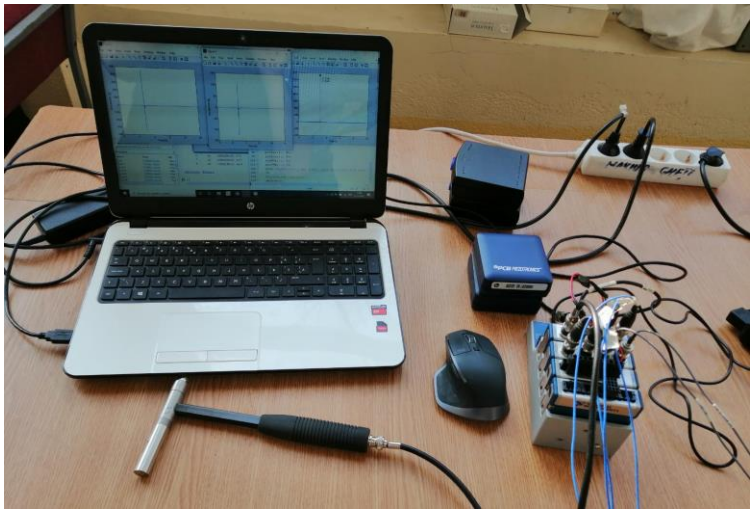

Fig. 3. Impact hammer, chassis and laptop.

The assembly is secured with 4 tightened bolts at the torque controlled according to the regulations. The rails – joint bars system has a gap of 7 mm length; the total length of test rig is 1203 mm.

A small steel piece is glued by the two railheads over the gap to allow the application of the hammer blow in the middle and the distribution of the impact force on the two rails. The system response is measured using two piezoelectric accelerometers (Bruel&Kjaer, type 4514) glued on both sides of the gap at the distance of 28 mm.

To put the system in vibration, an impact hammer (N.I., type PCB Modally Tuned®, model 086C03) with hard impact cap is used to cover a wide frequency range (fig. 3). Specialised chassis (NI cDAQTM-9174) is used for data acquisition. All data are managed by a laptop under MATLAB.

Fig. 4 shows the receptance of the rail calculated starting from the impact hammer force and the measured railhead accelerations. There are 3 diagrams from accelerometers and the mean diagram. There is a satisfactory reproducibility from a test to other one. It can be observed the peak at 33 Hz corresponding to the rigid mode of vibration of the rails on the elastic supports (bounce motion).

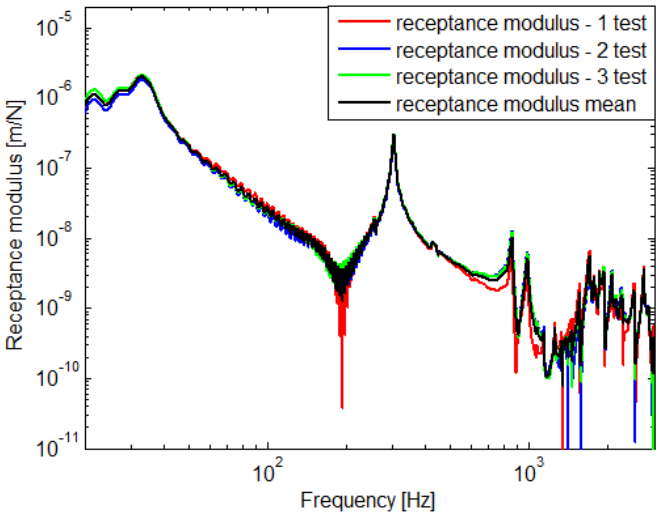

Fig. 4. Receptance modulus from tests.

Other peak is localised at 305 Hz and it is given by the first bending mode of the rails-joint bars system. This peak is preceded by a dip at around 194 Hz when the system experiences the antiresonance behaviour. At higher frequency there are many peaks and dips.

3. Mechanical model and equations of motion

Fig. 5 shows the mechanical model based on Euler-Bernoulli beam theory of the test rig. The model consists of three beams, of which two are identical and model the rails and the third beam models the joint bars. For generality, it is considered that the beams system is elastically supported at each end.

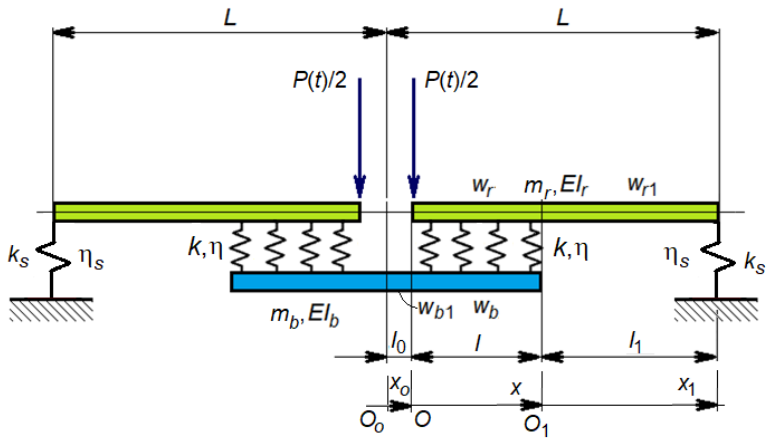

Fig. 5. Mechanical model of rails connected with joint bars.

Parameters for rails are: m_r – the mass per unit length, EI_r – the bending stiffness, where E is Young's modulus and I – the second moment of area of the cross-section and $l + l_1$ – the rails length. The joint bars have the following parameters: m_b – the mass per unit length, EI_b – the bending stiffness, where I_b is the second moment of area of the cross-section and $2\cdot(l_o + l)$ – the bars length. The connection between the rails and joint bars is modelled using Winkler elements of stiffness k with hysteretic damping of loss factor η. The supports have the stiffness k_s and the loss factor η_s.

The beams system is under the action of a harmonic force $P(t)$ of P_o amplitude and of ω angular frequency, $P(t) = P_o \cos \omega t$.

The harmonic force acts at the middle of the beams system, half on the right side and half on the left one. Next, only the right side of the beams system is considered due to symmetry reason.

The rail displacement is $w_r(x,t)$ for $0 \le x < l$ and $w_{r1}(x_1,t)$ for $0 \le x_1 < l_1$, and the bar displacement is $w_b(x,t)$ for $0 \le x < l$ and $w_{bo}(x_o,t)$ for $0 \le x_o < l_o$

To calculate the steady state harmonic behaviour of the beams system, the direct method is applied, and the input force and supports reaction are treated as boundary conditions. Also, boundary conditions must be imposed when the equation of motion changes as the section O for the jointed bar or the section O_1 for the rail, or at the ends beam.

Equations of motion are as follows:

- for $0 \le x < l$

$$\begin{aligned} EI_r \frac{\partial^4 w_r}{\partial x^4} + m_r \frac{\partial^2 w_r}{\partial t^2} + k\left(w_r - w_b\right) = 0 \\ EI_b \frac{\partial^4 w_b}{\partial x^4} + m_b \frac{\partial^2 w_b}{\partial t^2} + k\left(w_b - w_r\right) = 0 \end{aligned} \tag{1}$$

- for $0 \le x_1 < l_1$

$$EI_r \frac{\partial^4 w_{r1}}{\partial x_1^4} + m_r \frac{\partial^2 w_{r1}}{\partial t^2} = 0 \tag{2}$$

- for $0 \le x_o < l_o$

$$EI_b \frac{\partial^4 w_{b1}}{\partial x_o^4} + m_b \frac{\partial^2 w_{b1}}{\partial t^2} = 0\,, \tag{3}$$

where the arguments (x,t), (x_1,t) or (x_o,t) are missing due to the writing simplicity reasons.

Boundary conditions are as follows:

- for $x_o = 0$, the slope of the bars and the shear force are zero

$$\frac{\partial w_{b1}(0,t)}{\partial x_o} = 0; \qquad \frac{\partial^3 w_{b1}(0,t)}{\partial x_o^3} = 0; \tag{4}$$

- for $x_o = l_o$ and $x = 0$, the continuity conditions between w_{b1} and w_b

$$\frac{\partial^n w_{b1}(l_o,t)}{\partial x_o^n} = \frac{\partial^n w_b(0,t)}{\partial x^n} \text{ for } n = 0 \div 3; \tag{5}$$

- for $x = l$, the bending moment and shear force are zero

$$\frac{\partial^n w_b(l,t)}{\partial x^n} = 0 \text{ for } n = 2, 3; \tag{6}$$

- for $x = 0$, the bending moment is zero, and the shear force is $-P(t)/2$

$$\frac{\partial^2 w_r(0,t)}{\partial x^2} = 0, \qquad \frac{\partial^3 w_r(0,t)}{\partial x^3} = \frac{P(t)}{2EI_r}; \tag{7}$$

- for $x = l$ and $x_1 = 0$, the continuity conditions between w_r and w_{r1}

$$\frac{\partial^n w_r(l,t)}{\partial x^n} = \frac{\partial^n w_{r1}(0,t)}{\partial x_1^n} \text{ for } n = 0 \div 3; \tag{8}$$

- for $x_1 = l_1$ the bending moment is zero and the shear force is $-R(t)$, the reaction due to the elastic support

$$\frac{\partial^2 w_{r1}(l_1,t)}{\partial x_1^2} = 0, \qquad \frac{\partial^3 w_{r1}(l_1,t)}{\partial x_1^3} = \frac{R(t)}{EI_r}, \tag{9}$$

where $R(t) = k_s w_{r1}(l_1,t)$.

There are two limit cases, the support dynamic stiffness is zero (free-free)

$$\frac{\partial^2 w_{r1}(l_1,t)}{\partial x_1^2} = 0, \qquad \frac{\partial^3 w_{r1}(l_1,t)}{\partial x_1^3} = 0 \tag{9 a}$$

and the support stiffness is infinite (rigid support)

$$w_{r1}(l_1,t)=0,\quad \frac{\partial^2 w_{r1}(l_1,t)}{\partial x_1^2}=0\,. \tag{9b}$$

Now, considering the harmonic steady state behaviour, the following variables are introduced

$$\begin{aligned} &w_r(x,t)=W_r(x)\cos(\omega t+\varphi_r(x)) \quad w_{r1}(x_1,t)=W_{r1}(x_1)\cos(\omega t+\varphi_{r1}(x_1))\\ &w_b(x,t)=W_b(x)\cos(\omega t+\varphi_b(x)) \quad w_{b1}(x_o,t)=W_{b1}(x_o)\cos(\omega t+\varphi_{b1}(x_o)), \end{aligned} \tag{10}$$

where $W_r(x)$, $W_{r1}(x_1)$, $W_r(x)$, $W_{r1}(x_1)$ are the amplitude distributions and $\varphi_r(x)$, $\varphi_{r1}(x_1)$, $\varphi_r(x)$, $\varphi_{r1}(x_1)$ are the initial phase distributions along the beams system.

The following complex variables are associated to the real ones

$$\begin{aligned} &\bar{w}_r(x,t)=\bar{W}_r(x)e^{i\omega t} \quad \bar{w}_{r1}(x_1,t)=\bar{W}_{r1}(x_1)e^{i\omega t}\\ &\bar{w}_b(x,t)=\bar{W}_b(x)e^{i\omega t} \quad \bar{w}_{b1}(x_o,t)=\bar{W}_{b1}(x_o)e^{i\omega t}\\ &\bar{P}(t)=\bar{P}e^{i\omega t}, \end{aligned} \tag{11}$$

where the complex amplitude distributions are related to the real ones

$$\begin{aligned} &\bar{W}_r(x)=W_r(x)e^{i\varphi_r(x)} \quad \bar{W}_r(x_1)=W_r(x_1)e^{i\varphi_{r1}(x_1)}\\ &\bar{W}_b(x)=W_b(x)e^{i\varphi_b(x)} \quad \bar{W}_{b1}(x_o)=W_{b1}(x_o)e^{i\varphi_{b1}(x_o)}, \end{aligned} \tag{12}$$

and the complex amplitude of the harmonic force is $\bar{P}=P_o e^{i0}$, where i^2 = -1.

Corresponding to the Eqs. (1) – (3), it can be written

- for $0 \le x < l$

$$\begin{aligned} &EI_r\frac{\mathrm{d}^4\bar{W}_r}{\mathrm{d}x^4}+\bar{k}_r\bar{W}_r-\bar{k}\bar{W}_b=0\\ &EI_b\frac{\mathrm{d}^4\bar{W}_b}{\mathrm{d}x^4}+\bar{k}_b\bar{W}_b-\bar{k}\bar{W}_r=0 \end{aligned} \tag{13}$$

where $\bar{k}=k(1+i\eta)$ and $\bar{k}_{r,b}=\bar{k}-\omega^2 m_{r,b}$,

- for $0 \le x_1 < l_1$

$$\frac{\mathrm{d}^4 \bar{W}_{r1}}{\mathrm{d}x_1^4} - \beta_r^4 \bar{W}_{r1} = 0; \tag{14}$$

- for $0 \le x_o < l_o$

$$\frac{\mathrm{d}^4 \bar{W}_{b1}}{\mathrm{d}x_o^4} - \beta_b^4 \bar{W}_{b1} = 0, \tag{15}$$

where $\beta_{r,b} = \sqrt[4]{\dfrac{\omega^2 m_{r,b}}{EI_{r,b}}}$ are the wavenumber of the bending wave in the rail and joint bars, respectively.

Boundary conditions associated to the above equations of motion are:

- for $x_o = 0$, the slope of the bars and the shear force are zero (symmetry condition)

$$\frac{\mathrm{d}\bar{W}_{b1}(0)}{\mathrm{d}x_o} = 0; \quad \frac{\mathrm{d}^3 \bar{W}_{b1}(0)}{\mathrm{d}x_o^3} = 0; \tag{16}$$

- for $x_o = l_o$ and $x = 0$, the continuity conditions between w_{b1} and w_b

$$\frac{\mathrm{d}^n \bar{W}_{b1}(l_o)}{\mathrm{d}x_o^n} = \frac{\mathrm{d}^n \bar{W}_b(0)}{\mathrm{d}x^n} \quad \text{for } n = 0 \div 3; \tag{17}$$

- for $x = l$, the bending moment and shear force are zero

$$\frac{\mathrm{d}^n \bar{W}_b(l)}{\mathrm{d}x^n} = 0 \quad \text{for } n = 2, 3; \tag{18}$$

- for $x = 0$, the bending moment is zero and the shear force equals $-P(t)/2$

$$\frac{\mathrm{d}^2 \bar{W}_r(0)}{\mathrm{d}x^2} = 0, \quad \frac{\mathrm{d}^3 \bar{W}_r(0)}{\mathrm{d}x^3} = \frac{\bar{P}}{2EI_r}; \tag{19}$$

- for $x = l$ and $x_1 = 0$, the continuity conditions between w_r and w_{r1}

$$\frac{\mathrm{d}^n \bar{W}_r(l)}{\mathrm{d}x^n} = \frac{\mathrm{d}^n \bar{W}_{r1}(0)}{\mathrm{d}x_1^n} \text{ for } n = 0 \div 3; \tag{20}$$

- for $x_1 = l_1$ the bending moment is zero and the shear force is $-R(\mathrm{t})$, the reaction due to the elastic support

$$\frac{\mathrm{d}^2 \bar{W}_{r1}(l_1)}{\mathrm{d}x_1^2} = 0, \quad \frac{\mathrm{d}^3 \bar{W}_{r1}(l_1)}{\mathrm{d}x_1^3} = \frac{\bar{R}}{EI_r}, \tag{21}$$

where $\bar{R} = \bar{k}_s \bar{W}_{r1}(l_1)$ and $\bar{k}_s = k_s(1 + i\eta_s)$.

For the limit cases:

- free-free

$$\frac{\mathrm{d}^2 \bar{W}_{r1}(l_1)}{\mathrm{d}x_1^2} = 0, \quad \frac{\mathrm{d}^3 \bar{W}_{r1}(l_1)}{\mathrm{d}x_1^3} = 0; \tag{21 a}$$

- rigid support

$$\bar{W}_{r1}(l_1) = 0, \quad \frac{\mathrm{d}^2 \bar{W}_{r1}(l_1)}{\mathrm{d}x_1^2} = 0. \tag{21 b}$$

From Eqs. (13) it results

$$\begin{aligned} &EI_r EI_b \frac{\mathrm{d}^8 \bar{W}_r}{\mathrm{d}x^8} + \left(EI_r \bar{k}_b + EI_b \bar{k}_r\right) \frac{\mathrm{d}^4 \bar{W}_r}{\mathrm{d}x^4} + \left(\bar{k}_r \bar{k}_b - \bar{k}^2\right) \bar{W}_r = 0 \\ &\bar{W}_b = \frac{EI_r}{\bar{k}} \frac{\mathrm{d}^4 \bar{W}_r}{\mathrm{d}x^4} + \frac{\bar{k}_r}{\bar{k}} \bar{W}_r. \end{aligned} \tag{22}$$

Trying solutions of the following shape

$$\bar{W}_r(x) = W_r e^{\lambda x}, \tag{23}$$

the characteristic equation is obtained

$$EI_r EI_b \lambda^8 + \left(EI_r \bar{k}_b + EI_b \bar{k}_r \right) \lambda^4 + \left(\bar{k}_r \bar{k}_b - \bar{k}^2 \right) = 0$$
$$\bar{W}_b = \left(\frac{EI_r}{\bar{k}} \lambda^4 + \frac{\bar{k}_r}{\bar{k}} \right) \bar{W}_r . \tag{24}$$

Solving the first equation (24), it obtains

$$\bar{W}_r(x) = \sum_{i=1}^{8} A_i e^{\lambda_i x} \quad \bar{W}_b(x) = \sum_{i=1}^{8} \alpha_i A_i e^{\lambda_i x} , \tag{25}$$

where λ_i, $i = 1 \div 8$, are the eingenvalues and $\alpha_i = \left(EI_r \lambda_i^4 + \bar{k}_r \right) \bar{k}^{-1}$.

It can be shown that the solutions to Eqs. (14) and (15) are

$$\bar{W}_{r1}(x_1) = \sum_{i=1}^{4} A_{8+i} e^{\lambda_{ri} x_1} \quad \bar{W}_{b1}(x_o) = \sum_{i=1}^{4} A_{12+i} e^{\lambda_{bi} x_o} , \tag{26}$$

where λ_{ri} and λ_{bi} are the components of the vectors $\beta_{r,b} \cdot [1 \; -1 \; i \; -i]$.

Inserting (25) and (26) in the boundary conditions (16 – 21), it results

$$\sum_{i=1}^{4} \lambda_{bi} A_{12+i} = 0 ; \tag{27}$$
$$\sum_{i=1}^{4} \lambda_{bi}^3 A_{12+i} = 0 ; \tag{28}$$
$$\sum_{i=1}^{8} \alpha_i A_i - \sum_{i=1}^{4} A_{12+i} e^{\lambda_{bi} l_o} = 0 ; \tag{29}$$
$$\sum_{i=1}^{8} \lambda_i \alpha_i A_i - \sum_{i=1}^{4} \lambda_{bi} A_{12+i} e^{\lambda_{bi} l_o} = 0 ; \tag{30}$$
$$\sum_{i=1}^{8} \lambda_i^2 \alpha_i A_i - \sum_{i=1}^{4} \lambda_{bi}^2 A_{12+i} e^{\lambda_{bi} l_o} = 0 ; \tag{31}$$
$$\sum_{i=1}^{8} \lambda_i^3 \alpha_i A_i - \sum_{i=1}^{4} \lambda_{bi}^3 A_{12+i} e^{\lambda_{bi} l_o} = 0 ; \tag{32}$$
$$\sum_{i=1}^{8} \lambda_i^2 \alpha_i A_i e^{\lambda_i l} = 0 ; \tag{33}$$
$$\sum_{i=1}^{8} \lambda_i^3 \alpha_i A_i e^{\lambda_i l} = 0 ; \tag{34}$$

$$\sum_{i=1}^{8} \lambda_i^2 A_i = 0; \tag{35}$$

$$\sum_{i=1}^{8} \lambda_i^3 A_i = \frac{\bar{P}}{2EI_r}; \tag{36}$$

$$\sum_{i=1}^{8} A_i e^{\lambda_i l} - \sum_{i=1}^{4} A_{8+i} = 0; \tag{37}$$

$$\sum_{i=1}^{8} \lambda_i A_i e^{\lambda_i l} - \sum_{i=1}^{4} \lambda_{ri} A_{8+i} = 0; \tag{38}$$

$$\sum_{i=1}^{8} \lambda_i^2 A_i e^{\lambda_i l} - \sum_{i=1}^{4} \lambda_{ri}^2 A_{8+i} = 0; \tag{39}$$

$$\sum_{i=1}^{8} \lambda_i^3 A_i e^{\lambda_i l} - \sum_{i=1}^{4} \lambda_{ri}^3 A_{8+i} = 0; \tag{40}$$

$$\sum_{i=1}^{4} \lambda_{ri}^2 A_{8+i} e^{\lambda_{ri} l_1} = 0; \tag{41}$$

$$\sum_{i=1}^{4} \left(\lambda_{ri}^3 - \frac{\bar{k}_s}{EI_r} \right) A_{8+i} e^{\lambda_{ri} l_1} = 0. \tag{42}$$

For the limit cases, the equation (42) is replaced by:
for unsupported beam (free-free)

$$\sum_{i=1}^{4} \lambda_{ri}^3 A_{8+i} e^{\lambda_{ri} l_1} = 0; \tag{42 a}$$

for rigid support

$$\sum_{i=1}^{4} A_{8+i} e^{\lambda_{ri} l_1} = 0. \tag{42 b}$$

Solving the above algebraic systems of equations, the harmonic steady-state behaviour of the beams system can be studied.

3. Numerical application

In this section, the following values of the model parameters are considered: m_r = 49 kg/m, m_b = 42.5 kg/m, E = 210 GPa, $I_r = 18.19 \cdot 10^{-6}$ m^4, $I_b = 2 \cdot 1.635 \cdot 10^{-6}$ m^4, l_o = 3.5 mm, l = 304 mm and l_1 = 294 mm. The values parameters correspond to the 49 rail which is used at CFR (Romanian Railway).

In the first part of this section, some aspects regarding the influence of the stiffness and damping of the supports are addressed. The second part is dedicated to the identification of the parameters values of the rails - joint bars system based on the results of the measurement shown in Section 2.

Fig. 6 shows the receptance of the rail calculated next to the gap, considering undamped case. Three support stiffness values are considered: k_s= 2 MN/m^2 - continuous red line, k_s = 8 MN/m^2 – interrupted red line and k_s = 32 MN/m^2 – dotted red line. The limit cases are displayed too: free-free boundary conditions – green line, and rigid support ($k_s \to \infty$) – blue line. The stiffness of the rails-joint bars connection is k = 5.2 GN/m^2. Frequency ranges from 20 to 3000 Hz.

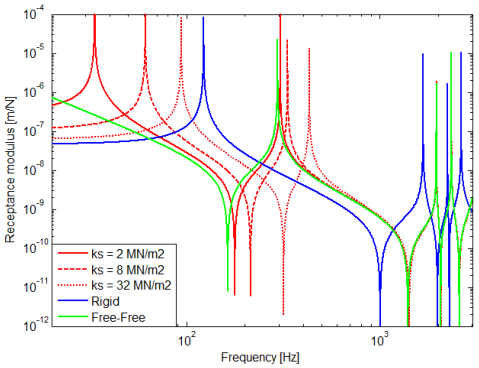

Fig. 6. Rail receptance – influence of the stiffness of the supports.

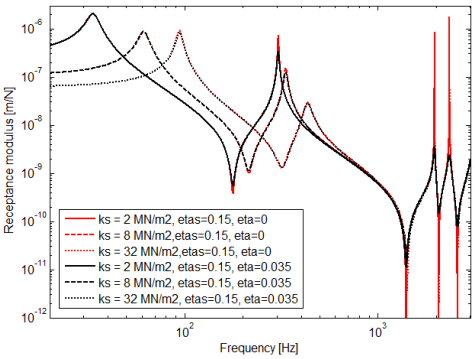

Fig. 7. Rail receptance – influence of the hysterertic damping.

At low frequency, the free-free beams system experiences the inertial behaviour and the receptance continuous decreases, and the beams system with rigid supports exhibits the elastic behaviour – receptance is constant (approximatively). The first resonance of the free-free beams system is at 296 Hz, while the system with rigid supports has the first resonance at 123 Hz. Higher resonances can be noted at 1959 and 2344 Hz for the free-free beams system and at 1674, 2230 and 2633 Hz for the system with rigid supports. When the elasticity of the supports is accounted for, the first resonance is lower than the one of the system fitted with rigid supports, but its second resonance is higher than the first resonance of the free-free beams system. Decreasing the supports stiffness, the first two resonances becomes lower. At high frequency, the stiffness of the supports has little influence on the rail receptance for the three values considered here and the rail behaviour is similar with the one of the free-free beams system.

Figure 7 presents the rail receptance calculated next to the gap using only the elastic support model ($k_s \in \{2$ MN/m^2, 8 MN/m^2, 32 MN/m$^2\}$), considering the hysteretic damping for both supports and rail-joint bar connection. The loss factor

is 0.15 for the supports damping and the loss factor of 0.035 is for the rails-joint bars connection.

It can be observed the three red lines which correspond to the rail receptance calculated for $\eta_s = 0.15$ and $\eta = 0$. It results that the supports damping influences strongly the rail response at the first two resonances, but this has very little influence on the higher resonances.

The three black lines show the rail receptance calculated when the damping of the rails-joint bars connection is considered ($\eta_s = 0.15$ and $\eta = 0.035$). It results that the damping of the rails-joint bars connection has strong influence on the higher resonances and significant influence on the second resonance; this observation is for $\eta = 0.035$. On the other hand, the damping of the rails-bars connection has no influence on the first resonance.

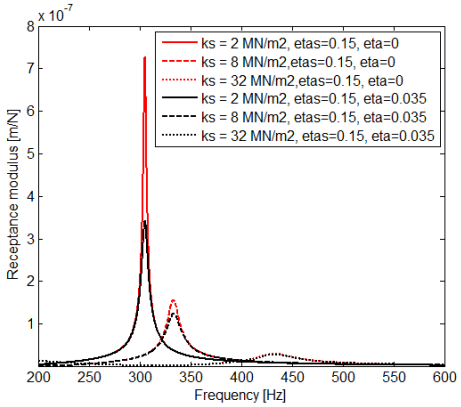

Fig. 8. Rail receptance – influence of the hysterertic damping (detail).

It is interesting what happens at the second resonance (fig. 8). The supports damping and the one of the rails-joint bars connection lead to rail receptance limitation. From this point of view, it is important to identify the parameters configuration allowing to evidence the influence of the rails-joint bars connection damping which is much lower than the supports damping. Only that parameters configuration is proper to assess the damping of the rails-joint bars connection via measurements. Diagrams in Fig. 8 show that when the support stiffness is high (k_s = 32 MN/m2), the influence of the damping of the rails-joint bars connection is practically undetectable. Situation is somehow improved for k_s = 8 MN/m^2, but this becomes very promising when the soft supports are used in calculation (k_s = 2 MN/m^2).

It should be emphasized that this observation was the basis for the design of the rail joint test rig (Section 2).

Figure 9 a shows the receptance of the rail calculated for the undamped case at 28 mm from the gap and the receptance of the rail obtained from measurement; the distance of 28 mm from the gap corresponds to the

accelerometers position. The stiffness of the supports is k_s = 2 MN/m and the stiffness of the connection between rails and joint bars is k = 5.2 GN/m^2. There is good agreement between the predicted receptance and the measured one up to 6-700 Hz, excepting the receptance at the first two resonances due to the lack of damping in the theoretical model. At higher frequency, the dynamic behaviour has more peaks and deeps then those predicted by the above model.

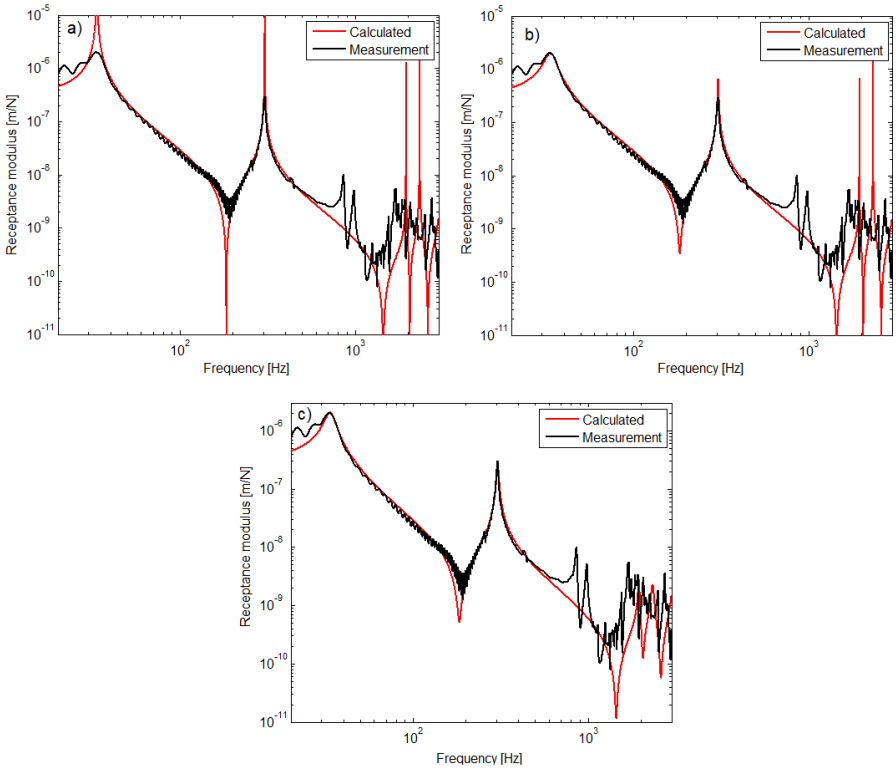

Fig. 9. Predicted rail receptance at 28 mm from the gap vs. measured rail receptance: a) $\eta_s = \eta = 0$; b) $\eta_s = 0.15$, $\eta = 0$; c) $\eta_s = 0.15$, $\eta = 0.035$.

Next step, the hysteretic damping is considered. First, the damping of the support is 'accorded' with the measured data. Fig. 9 b presents the rail receptance when the loss factor of the supports is 0.15, and the loss factor of the rails-joint bars connection is zero. In this case, the agreement between the predicted and measured receptance is very good even at the first resonance of 33 Hz, but a discrepancy can be observed at the second resonance.

Finally, the damping of the rails-joint bars connection is fitted according to the measured data at the second resonance. Figure 9 c shows the rail receptance when both damping of the supports and rails-joint bars connection are taken for (η_s = 0.15 and η =0.035). The discrepancy is vanished.

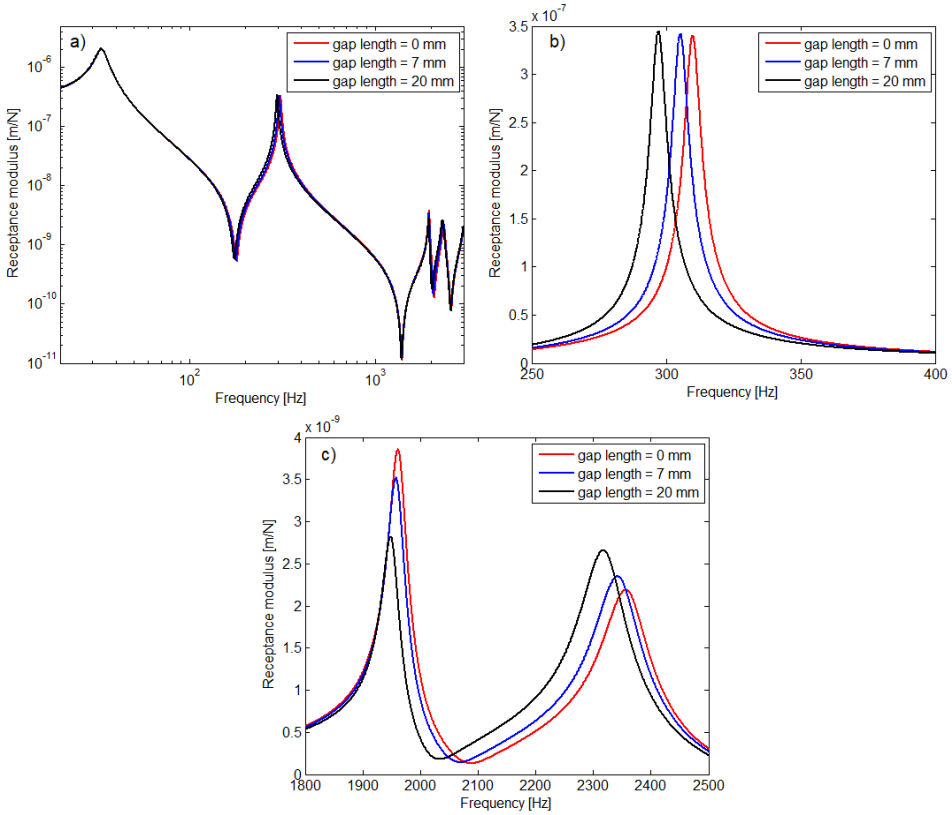

Fig. 10. Influence of the gap length on the rail receptance:
a) 20 – 3000 Hz; b) 250 – 400 Hz;c) 1800-2500 Hz.

Figure 10 shows the rail receptance next to the gap for three values of the gap length: 0, 7 and 20 mm. When the gap length increases, the rail joint becomes more elastic and the resonance frequencies decrease. This tendency can be observed at all resonance frequencies. For instance, the resonance frequency decreases by 13 Hz at the second resonance, 12 Hz at the third resonance, and 40 Hz at the third resonance. Rail receptance has little variation at the second resonance, 1%. Higher variation can be noticed at the third resonance (decrease of 27 %) and the fourth resonance (increase of 17 %) when the gap length passes from 0 to 20 mm.

6. Conclusions

In this paper, the model of the rail joint test rig, consisting of two rails connected by two joint bars and bolts, elastically supported at the ends, is elaborated and used to point out the influence of elastic supports on the dynamic behaviour of the rail joint. The model is based on the Euler-Bernoulli beam theory and includes two beams for the rails and an equivalent beam for the two joint bars.

Rails – joint bars connection is modelled using Winkler foundation with hysteretic damping.

The resonances of the model are pointed out and it is shown that the hysteretic damping of the supports influences the first two resonances, and the hysteretic damping of the rails–joint bars connection influences the second resonance and the higher resonances. The impact of the damping of the rails-joint bars connection on the rail response at the second resonance is increasing when the softer supports are used. This important result has been used to design the rail joint test rig.

Rail response in terms of receptance has been obtained using the rail joint test rig by applying the impact hammer method. The stiffness and hysteretic of the supports and rails-joint bars connection has been determined based on the comparison between the theoretical and experimental results.

The proposed model can be applied up to 6-700 Hz and should be used to predict the interaction between the wheelset and jointed track.

The gap length has little influence on the rail response at the second resonance: the resonance frequency decreases by 13 Hz and the receptance modulus increases by 1 %, when the gap length increases from 0 to 20 mm.

Acknowledgment

This work has been funded by the European Social Fund from the Sectoral Operational Programme Human Capital 2014-2020, through the Financial Agreement with the title "Scholarships for entrepreneurial education among doctoral students and postdoctoral researchers (Be Antreprenor!)", Contract no. 51680/09.07.2019 - SMIS code: 124539, project in which the co-authors Marius-Alin Gheți and Mihai-Cornel Leu participate.

R E F E R E N C E S

[1] 314 Instruction, Rules and tolerances for track construction and maintenance, 1989.

[2] *S.K. Samantaraya, S.K. Mittala, P. Mahapatra, S. Kumar*, Assessing the flexion behavior of bolted rail joints using finite element analysis, Engineering Failure Analysis, **vol**. **104**, 2019, pp. 1002-1013.

[3] *Z. Yanga, A. Boogaard, R. Chen, R. Dollevo, Z. Li*, Numerical and experimental study of wheel-rail impact vibration and noise generated at an insulated rail joint, International Journal of Impact Engineering, **vol**. **113**, 2018, pp. 29–39.

[4] *W. Cai, Z. Wen, X. Jin, W. Zhai*: Dynamic stress analysis of rail joint with height difference defect using finite element method, Engineering Failure Analysis, **vol**. **14**, 2007, pp. 1488-1499.

[5]. *Y. C. Chen, L.W. Chen*, Effects of insulated rail joint on the wheel/rail contact stresses under the condition of partial slip, Wear, **vol. 260**, 2006, pp. 1267-1273.

[6]. *M. Oregui*, Vertical Railway Track Dynamics: From Measurements to Numerical Modelling, PhD Thesis, Technische Universiteit Delft, 2015.